Liquid Crystals
Publication details, including instructions for authors and subscription information:
http://www.informaworld.com/smpp/title~content=t713926090

Experimental study of a SmA*-SmC*$_A$ phase transition

S. Sarmento; M. R. Chaves; P. Simeão Carvalho; H. T. Nguyen

Online publication date: 06 August 2010

To cite this Article Sarmento, S. , Chaves, M. R. , Carvalho, P. Simeão and Nguyen, H. T.(2001) 'Experimental study of a SmA*-SmC*$_A$ phase transition', Liquid Crystals, 28: 10, 1561 — 1571
To link to this Article: DOI: 10.1080/02678290110068415
URL: http://dx.doi.org/10.1080/02678290110068415

LIQUID CRYSTALS, 2001, VOL. 28, NO. 10, 1561–1571

Experimental study of a SmA*–SmC$^*_A$ phase transition

S. SARMENTO, M. R. CHAVES*, P. SIMEÃO CARVALHO
Departamento de Física, IFIMUP, CFUP,
Faculdade de Ciências da Universidade do Porto, Rua do Campo Alegre 687,
4169-007 Porto, Portugal

and H. T. NGUYEN
Centre de Recherche Paul Pascal, Av. A. Schweitzer, 33600 Pessac, France

(*Received 27 December 2000; in final form 6 March 2001; accepted 16 March 2001*)

We have performed a detailed experimental study of the electroclinic behaviour in the SmA* phase above a SmA*–SmC$^*_A$ phase transition. The tilt angle and polarization were measured as a function of the applied a.c. electric field, and the dielectric constant was obtained under different values of the bias field ($0 \leqslant E_{d.c.} \leqslant 3$ V μm^{-1}). In the region of linear regime, the behaviour observed for this SmA*–SmC$^*_A$ phase transition is very similar to the one previously described for SmA*–SmC* phase transitions. The experimental results obtained under high bias field are in good agreement with the predictions of the simple theoretical model considered.

1. Introduction

Liquid crystals presenting the SmC$^*_A$ phase are traditionally called antiferroelectrics [1]. Antiferroelectric liquid crystals may be described by a Landau expansion of the free energy in the order parameters [2]: $\xi_a = (\xi_i - \xi_{i+1})/2$, $\xi_f = (\xi_i + \xi_{i+1})/2$, where $\xi_i = (n_{i_x} n_{i_z}, n_{i_y} n_{i_z})$† and $n_i = (n_{i_x}, n_{i_y}, n_{i_z})$ is the director of the ith layer. These materials may present several different phase sequences, of which we list the three following examples:

(1) I–SmA*–SmC$^*_A$–Cr
(2) I–SmA*–SmC*–SmC$^*_{FI}$–SmC$^*_A$–Cr
(3) I–SmA*–SmC$^*_\alpha$–SmC*–SmC$^*_{FI}$–SmC$^*_A$–Cr

The first type of phase sequence provides a nice opportunity to check simple theoretical models, avoiding recent dicussions over the structure of ferrielectric phases [3, 4]. The direct SmA*–SmC$^*_A$ phase transition was first studied by Hiraoka *et al.* [5], by dielectric measurements with no applied bias field. These authors were mostly concerned with the comparison between 1st and 2nd order transitions.

In this work, we have studied experimentally the behaviour of the ferroelectric amplitude mode in the SmA* phase of a liquid crystal presenting the SmA*–SmC$^*_A$ phase transition. The aim of this paper is to compare this phase transition with the classical SmA*–SmC* transition, which has been studied previously [6, 7]. The dielectric response in the SmA* phase without d.c. field should be similar in both cases, as the equations describing the electroclinic effect (linear coupling of the electric field to the ferroelectric order parameter) and the dynamics of the ferroelectric amplitude mode, are the same. There is, however, a fundamental difference in the coupling of the electric field to the order parameter that becomes non-zero in the low temperature phase. The electric field couples linearly to ξ_f and quadratically to ξ_a. We have found that dielectric measurements under high d.c. bias field can reveal some interesting details of the SmA*–SmC$^*_A$ phase transition. For the present study we have chosen a newly synthesized tolane. It presents a direct SmA*–SmC$^*_A$ phase transition and also a strong electroclinic effect. The chemical formula is [8]:

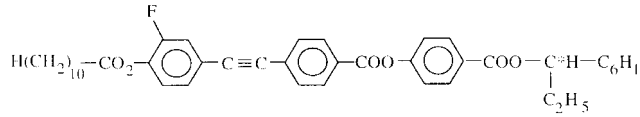

According to preliminary differential scanning calorimetry (DSC) measurements and texture observations, the phase sequence is:

$$\text{Cr} \xrightarrow{36^\circ\text{C}} \text{SmC}^*_A \xrightarrow[(0.08\ \text{kJ mol}^{-1})]{40^\circ\text{C}} \text{SmA} \xrightarrow[(2.3\ \text{kJ mol}^{-1})]{67^\circ\text{C}} \text{I}.$$

*Author for correspondence; e-mail: rachaves@fc.up.pt
† In reference [2], the authors considered $\xi_i = (-n_{i_y} n_{i_z}, n_{i_x} n_{i_z})$.

Liquid Crystals ISSN 0267-8292 print/ISSN 1366-5855 online © 2001 Taylor & Francis Ltd
http://www.tandf.co.uk/journals
DOI: 10.1080/02678290110068415

We have performed a detailed experimental study of the electroclinic behaviour in the SmA* phase, including tilt angle (θ) and polarization measurements, as a function of the electric field. The results obtained are presented and compared with those of Glogarová *et al.* [6] for a SmA*–SmC* phase transition. Measurements of the dielectric constant ($\varepsilon^* = \varepsilon' + i\varepsilon''$) as a function of the applied bias field ($0 \leqslant E_{d.c.} \leqslant 3\ V\ \mu m^{-1}$) revealed that both the maximum value of ε' (ε'_{max}) and the temperature where it occurs (T_{max}) depend on the applied d.c field, $E_{d.c.}$. We will use a simple theoretical model, derived from the Landau expansion originally proposed by Orihara and Ishibashi [3], to explain qualitatively the observed dependence of ε'_{max} and T_{max} with $E_{d.c.}$.

2. Theoretical model

2.1. *Equilibrium situation (no electric field applied)*

The very low transition enthalpy of the SmA*–SmC$^*_A$ phase transition and its small thermal hysteresis (≈ 0.2°C) suggest that the relevant parameters change in an almost continuous way. Therefore it seems unnecessary to include 6th order terms in the free energy, as the phase transition is not markedly first order.

As pointed out by Beaubois *et al.* [9], the two order parameters are related by $\xi_a^2 + \xi_f^2 \approx \theta^2$. This relation and the calorimetry measurements of Ema *et al.* [10] suggest that the two order parameters are not independent and that there is only one Curie temperature, T_o. The electro-optical results of Beaubois *et al.* [9] support this hypothesis. The Landau expansion of the free energy can therefore be written [2, 11–13]:

$$\begin{aligned} f = {} & \frac{1}{2}a(\xi_a^2 + \xi_f^2) + \frac{1}{2}a'(\xi_f^2 - \xi_a^2) + \frac{1}{4}b_a\xi_a^4 \\ & + \frac{1}{4}b_f\xi_f^4 + \frac{1}{2}\gamma_1\xi_a^2\xi_f^2 + \frac{1}{2}\gamma_2(\xi_a\ \ \xi_f)^2 \\ & - \Lambda_a\left[\xi_{a_x}\frac{\partial\xi_{a_y}}{\partial z} - \xi_{a_y}\frac{\partial\xi_{a_x}}{\partial z}\right] - \Lambda_f\left[\xi_{f_x}\frac{\partial\xi_{f_y}}{\partial z} - \xi_{f_y}\frac{\partial\xi_{f_x}}{\partial z}\right] \\ & + \frac{1}{2}K_a\left[\left(\frac{\partial\xi_{a_x}}{\partial z}\right)^2 + \left(\frac{\partial\xi_{a_y}}{\partial z}\right)^2\right] \\ & + \frac{1}{2}K_f\left[\left(\frac{\partial\xi_{f_x}}{\partial z}\right)^2 + \left(\frac{\partial\xi_{f_y}}{\partial z}\right)^2\right] \end{aligned} \tag{1}$$

where only the coefficient $a = \alpha(T - T_o)$ is temperature dependent.

Due to the helicoidal structure of the SmC$^*_A$ phase, we may write: $\xi_a = \xi_a[\cos(qz), \sin(qz)]$. As pointed out by Žekš, $\xi_a\ \ \xi_f = 0$ minimizes the free energy when the coupling constant γ_2 is positive. Due to the definitions of ξ_a and ξ_f, the condition $\xi_a\ \ \xi_f = 0$ is always satisfied under the constraint of constant tilt angle [9]. Therefore, in the following we will consider ξ_a perpendicular to ξ_f and write:

$$\xi_f = \xi_f[-\sin(qz), \cos(qz)].$$

Finally, expansion (1) can be written:

$$f = \frac{1}{2}\tilde{\alpha}_a\xi_a^2 + \frac{1}{4}b_a\xi_a^4 + \frac{1}{2}\tilde{\alpha}_f\xi_f^2 + \frac{1}{4}b_f\xi_f^4 + \frac{1}{2}\gamma_1\xi_a^2\xi_f^2 \tag{2}$$

where:

$$\begin{aligned} \tilde{\alpha}_a &= \alpha(T - T_a) + K_a q^2 - 2\Lambda_a q \\ \tilde{\alpha}_f &= \alpha(T - T_f) + K_f q^2 - 2\Lambda_f q \\ T_a &= T_o + \frac{a'}{\alpha} \\ T_f &= T_o - \frac{a'}{\alpha} \end{aligned}$$

$$\begin{cases} \dfrac{\partial f}{\partial\xi_a} = \tilde{\alpha}_a\xi_a + \gamma_1\xi_f^2\xi_a + b_a\xi_a^3 \\ \dfrac{\partial^2 f}{\partial\xi_a^2} = \tilde{\alpha}_a + \gamma_1\xi_f^2 + 3b_a\xi_a^2 \end{cases} \tag{3}$$

The system under study presents the direct SmA*–SmC$^*_A$ phase transition, therefore in equilibrium $\xi_f = 0$ at all temperatures.

$$T > T_c = T_a + \frac{2\Lambda_a q - K_a q^2}{\alpha} \Rightarrow \begin{cases} \xi_a = 0 \\ \xi_f = 0 \end{cases}$$

$$T < T_c = T_a + \frac{2\Lambda_a q - K_a q^2}{\alpha} \Rightarrow \begin{cases} \xi_a^2 = -\dfrac{\alpha}{b_a}(T - T_c) \\ \xi_f = 0 \\ q = \dfrac{\Lambda_a}{K_a} \end{cases}$$

In a helicoidal sample, the phase transition SmA*–SmC$^*_A$ occurs at the temprature $T_c > T_a$. Without the helicoidal structure, the transition would occur at the lower temperature, T_a.

According to Žekš and Čepič [11], we may expect two amplitude modes in the SmA* phase, one ferroelectric and the other antiferroelectric (the antiferroelectric amplitude mode does not contribute to the dielectric constant and therefore will not be considered in the model). The two amplitude modes go soft at different temperatures. If the ferroelectric amplitude

mode condenses at higher temperatures than the antiferroelectric amplitude mode ($T_f > T_a$), the SmA*–SmC* phase transition occurs. If the reverse is true ($T_f < T_a$), the SmA*–SmC^*_A phase transition takes place.

2.2. *The SmA* phase under an applied electric field*

There is no equilibrium helical structure in the SmA* phase. Assuming that the electric field is spatially uniform, derivatives with respect to z may be neglected.

In the SmA* phase, the equilibrium values of ξ_a and ξ_f are null. Their induced values, $\Delta\xi_a$ and $\Delta\xi_f$, are proportional, respectively, to the square of the electric field and to the field itself [13]: $\Delta\xi_a \propto E^2$, $\Delta\xi_f \propto E$. Here we will consider linear coupling to the electric field. Consequently, if the electric field is applied along the xx direction, $\mathbf{E} = Ee_x$, the Landau expansion to be considered in the SmA* phase is

$$f(\text{field}) = f + C_f(P_x\xi_{f_y} - P_y\xi_{f_x}) + \frac{(P_x^2 + P_y^2)}{2\varepsilon_o\chi_f} - \mathbf{P}\ \ \mathbf{E}$$

$$\frac{\partial f(\text{field})}{\partial \mathbf{P}} = 0 \Rightarrow \begin{cases} P_x = \varepsilon_o\chi_f(-C_f\xi_{f_y} + E) \\ P_y = \varepsilon_o\chi_f C_f \xi_{f_x} \end{cases} \tag{4}$$

The applied electric field will induce a polarization along the xx direction, $\mathbf{P} = \Delta P \mathbf{e}_x$. Due to the C_f term, a small uniform tilt angle will also be induced by the electric field (electroclinic effect), implying $\xi_f \neq 0$. The plane where the molecules tilt will be perpendicular to $\mathbf{P}$.

We may write:

$$\boldsymbol{\xi}_f = \xi_{f_y} e_y = -\Delta\xi_f e_y \quad \boldsymbol{\xi}_a = \Delta\xi_a e_x$$

$$\begin{aligned} f(\text{field}) = {} & \frac{1}{2}\alpha(T - T_a)\Delta\xi_a^2 + \frac{1}{4}b_a\Delta\xi_a^4 + \frac{1}{2}\alpha(T - T_S)\Delta\xi_f^2 \\ & + \frac{1}{4}b_f\Delta\xi_f^4 + \frac{1}{2}\gamma_1\Delta\xi_a^2\Delta\xi_f^2 - \frac{1}{2}\varepsilon_o\chi_f E^2 \\ & - \varepsilon_o\chi_f C_f\Delta\varepsilon_f E \\ \approx {} & \frac{1}{2}\alpha(T - T_a)\Delta\xi_a^2 + \frac{1}{2}\alpha(T - T_S)\Delta\xi_f^2 + \frac{1}{4}b_f\Delta\xi_f^4 \\ & - \frac{1}{2}\varepsilon_o\chi_f E^2 - \varepsilon_o\chi_f C_f\Delta\xi_f E \end{aligned} \tag{5}$$

where $T_S = T_f + \varepsilon_o\chi_f C_f^2/\alpha$. We have retained terms only up to the fourth order in E.

2.2.1. *Low electric field and linear response*

For weak electric fields, it is sufficient to retain only quadratic terms in E in the expansion (5) ($b_f\Delta\xi_f^4 \approx 0$). In the region of linear electroclinic response, $\theta = eE$ (e = electroclinic coefficient); we can perform the same study that Glogarová *et al.* [6] did for a family of compounds presenting the SmA*–SmC* phase transition. The relations that can be verified experimentally are:

$$\frac{\partial f(\text{field})}{\partial\Delta\xi_f} = 0 \Rightarrow \Delta\xi_f = \frac{\varepsilon_o\chi_f C_f}{\alpha(T - T_S)}E = eE \tag{6}$$

$$\text{equations (4) and (6)} \Rightarrow P_x = \varepsilon_o\left[\frac{\varepsilon_o(\chi_f C_f)^2}{\alpha(T - T_S)} + \chi_f\right]E \tag{7}$$

$$\left.\begin{aligned} -\frac{\partial f}{\partial(\Delta\xi_f)} &= \gamma\frac{\partial(\Delta\xi_f)}{\partial t} \\ [E = E_o\exp(i\omega t)] & \end{aligned}\right\} \Rightarrow \varepsilon^* = \chi_f + \frac{\Delta\varepsilon_S}{1 + i\dfrac{\omega}{\omega_R}} \tag{8}$$

$$\omega_R = \frac{\alpha(T - T_S)}{\gamma}, \quad T > T_S$$

$$\Delta\varepsilon_S = \frac{\varepsilon_o(\chi_f C_f)^2}{\alpha(T - T_S)}, \quad T > T_S.$$

The amplitude mode presents a Curie–Weiss behaviour in the SmA* phase, according to relation (8). However, its softening occurs at the temperature T_S, not at the temperature T_c where the phase transition occurs.

2.2.2. *Measurements with an applied bias field*

When dielectric measurements are performed under an applied bias field, the total electric field may be written as $\mathbf{E}_{total} = [E_{d.c.} + E_o\exp(i\omega t)]e_x$, with $E_o \ll E$. Consequently, the induced ferroelectric parameter may also be written as: $\Delta\xi_{f_{total}} = \Delta\xi_f + \delta\xi_f\exp(i\omega t)$, with $\Delta\xi_f \gg \delta\xi_f$. Introducing these expressions in the expansion (5), where the 4th order terms are no longer small, we obtain:

$$\begin{aligned} \gamma\frac{\partial\Delta\xi_{f_{total}}}{\partial t} &= -\frac{\partial f(\text{field})}{\partial\Delta\xi_{f_{total}}} \\ -i\omega\gamma\delta\xi_f\exp(i\omega t) &= \alpha(T - T_S)(\Delta\xi_f + \delta\xi_f\exp(i\omega t)) \\ & \quad + b_f(\Delta\xi_f)^2(\Delta\xi_f + 3\delta\xi_f\exp(i\omega t)) \\ & \quad - \varepsilon_o\chi_f C_f(E_{d.c.} + E_o\exp(i\omega t)) \\ & \quad + O(\delta\xi_f^2) \end{aligned}$$

The time independent part of this equation gives the equilibrium condition:

$$\alpha(T - T_S)\Delta\xi_f + b_f(\Delta\xi_f)^3 - \varepsilon_o\chi_f C_f E = 0. \tag{9}$$

From the time-dependent part we obtain the dielectric contribution and relaxation frequency of the ferroelectric amplitude mode as:

$$\Delta\varepsilon_S = \frac{\varepsilon_o(\chi_f C_f)^2}{\alpha(T - T_S) + 3b_f(\Delta\xi_f)^2} \tag{10}$$

$$\omega_R = \frac{\alpha(T - T_S) + 3b_f(\Delta\xi_f)^2}{\gamma}. \tag{11}$$

According to Glogarová and Pavel [7], the maximum contribution to the dielectric constant, $\Delta\varepsilon'_{max}$, will occur at a temperature $T_{max} = T_S + \Delta T_{max}$. Close to T_S,

$$\frac{1}{\Delta\varepsilon'_{max}} \propto \Delta T_{max} \propto E^{2/3}. \quad (12)$$

This was verified experimentally for a SmA*–SmC* phase transition [7], but in the limit of sufficiently high field to unwind the helix, as the Goldstone mode hides the contribution from the soft mode.

In the case of a SmA*–SmC$^*_A$ transition the maximum dielectric contribution of the amplitude mode is visible even without bias field, as the helicoidal structure of the SmC$^*_A$ phase is associated only with weak relaxation processes.

3. Experimental

The liquid crystals were filled by capillarity into commercial cells (E. H. C. Co, Japan), coated with ITO electrodes and rubbed polyimide. Measurements were made on planar samples of thickness 25 and 3 μm. As there was total agreement between the results obtained for samples of different thickness, we have preferred to use the 3 μm thick samples for the dielectric measurements under bias field.

The samples were placed in a specially built oven and the temperature was controlled with a Lakeshore DRC-93CA temperature controller, using a chromel alumel thermocouple as a thermometer. The accuracy was better than 0.1 K.

The dielectric constant was measured at stabilized temperatures on cooling and heating, in the frequency range 20 Hz–1 MHz, using a HP4284A LCR meter. The resistance of the electrodes in series with the liquid crystal sample mimics a false relaxation mode (ITO effect) around 1 MHz [14].

The dielectric data were fitted to the expression:

$$\varepsilon^*(\omega) = \varepsilon(\infty) + \sum_j \frac{\Delta\varepsilon_j}{1 + \left(i\frac{f}{f_{R_j}}\right)^{\beta_j}} \quad (13)$$

where $\Delta\varepsilon_j$, f_{R_j} and β_j are, respectively, the dielectric amplitude, relaxation frequency and dispersion parameter of the j-th mode.

Measurements of the low frequency dielectric constant, as a function of the applied bias field, were performed using a HP4192A or, alternatively, an Ando AG4311. Optical and polarization hysteresis loops were obtained using a HP33120A signal generator and a Kepko (Bop 1000M) signal amplifier. The intensity of the transmitted light was measured with a BPW21 (R.S. Components, Ltd.) photodiode.

4. Experimental results and discussion

In the SmC$^*_A$ phase, two dielectric relaxation processes are present. Because of their small dielectric amplitudes and high relaxation frequencies, it is impossible to characterize them accurately in the presence of the ITO effect. Figure 1 shows typical dielectric dispersion curves in the SmC$^*_A$ and SmA* phases of C10(F)Tolane. In the SmA* phase, only one relaxation mode is detected. This is the ferroelectric amplitude mode, usually called the soft mode. Its dielectric amplitude increases and its relaxation frequency decreases as the phase transition is approached.

The SmA*–SmC$^*_A$ phase transition occurs at the temperature T_c and is accompanied by a change of texture (as observed by polarizing optical microscopy) and an abrupt decrease of the I_{zz} normalized Raman intensity [15]. It was observed that the maximum value of the dielectric constant is also attained at the transition temperature T_c. This happens because $T_c > T_S$, so that the Curie–Weiss behaviour of the amplitude mode is interrupted by the phase transition at T_c. If the phase transition did not take place the maximum dielectric contribution of the soft mode would occur at T_S, according to relations (6) and (8).

Figure 2 shows the real part of the dielectric constant, obtained at 1 kHz, on cooling and heating runs. There is a small thermal hysteresis of the phase transition: T_c (cooling) = 40.3°C and T_c (heating) = 40.5°C, for a 3 μm thick sample. In the following discussion we will use the relative temperature $T - T_c$, where T_c = 40.5°C on heating runs and T_c = 40.3°C on cooling runs, for a 3 μm thick sample. For 25 μm thick samples, slightly different transition temperatures were obtained: T_c (cooling) = 39.7°C and T_c (heating) = 39.9°C, for a 25 μm thick sample.

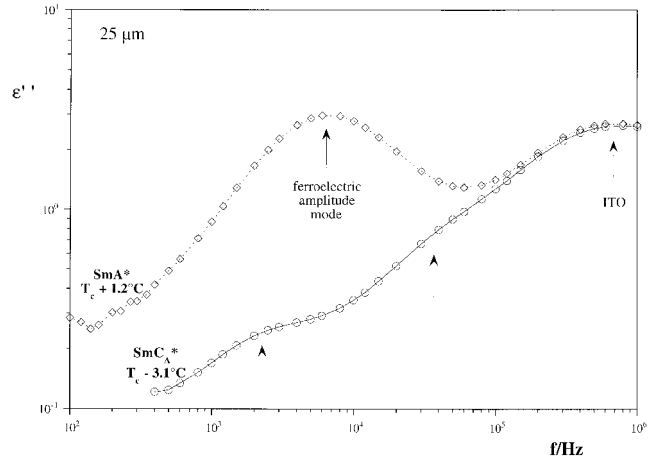

Figure 1. Imaginary part of the dielectric constant, as a function of the frequency, measured at stabilized temperature in the SmC$^*_A$ and SmA* phases.

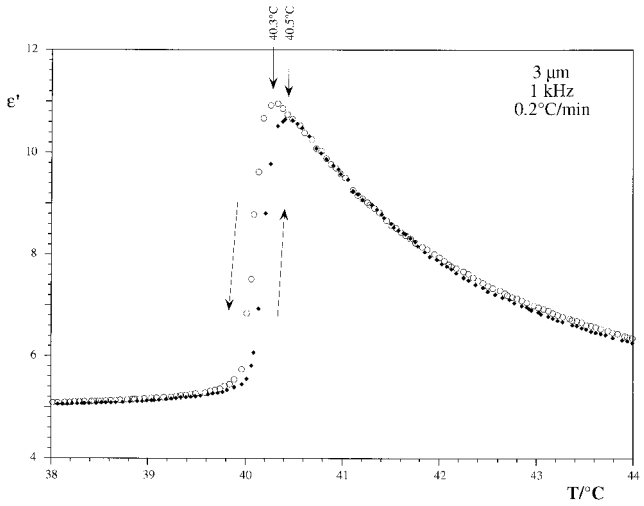

Figure 2. Real part of the dielectric constant, measured at 1 kHz on cooling and heating runs, for a 3 µm thick sample. This curve is very similar to the one obtained by Hiraoka *et al.* [5], for the compound (*S*)-TFMHPOBC.

Dielectric dispersion data were obtained at several stabilized temperatures, on cooling and heating runs. Figures 3 and 4 show the temperature dependence of f_R and $1/\Delta\varepsilon$, near the phase transition, for 25 and 3 µm thick samples, respectively. From the linear fits to the experimental data presented in figures 3 and 4, we may conclude that the temperature T_S is approximately 1–1.3°C lower than T_c.

Bourny *et al.* [16] have introduced an original way for verifying the Curie–Weiss behaviour of the amplitude mode. Instead of obtaining the relaxation frequency from the fit of equation (13), their method consists in determining the temperature, T_m, where the maximum of the real part of the dielectric constant occurs.

Assuming perfect Debye behaviour of the amplitude mode, the contribution of this relaxation process to the real part of the dielectric constant is written as:

$$\varepsilon' = Re\left(\frac{\Delta\varepsilon_S}{1+\mathrm{i}\dfrac{\omega}{\omega_R}}\right) = \frac{\Delta\varepsilon_S}{1+\left(\dfrac{\omega}{\omega_R}\right)^2}$$

where $\Delta\varepsilon_S$ and ω_R are given as in relation (8). We may distinguish two situations. In low frequency dielectric measurements, $\omega \ll \omega_R$, the real part of the dielectric constant reflects only the temperature dependence of $\Delta\varepsilon_S$ and presents a maximum at $T = T_c$. For C10(F) tolane this behaviour was still observed for $f = \omega/2\pi = 1$ kHz, as shown in figure 2.

For $\omega \geqslant \omega_R$, the function $\varepsilon'(T)$ presents a maximum at the temperature T_m given by (see appendix A):

$$T_m = T_S + \frac{2\pi\gamma}{\alpha} \times f. \qquad (14)$$

According to relation (14), in the case of Curie–Weiss behaviour, T_m should vary linearly with the measuring frequency, f.

The results obtained for a 3 µm thick sample with this alternative method are presented in figure 5. They agree very well with those presented in figure 4. The advantage

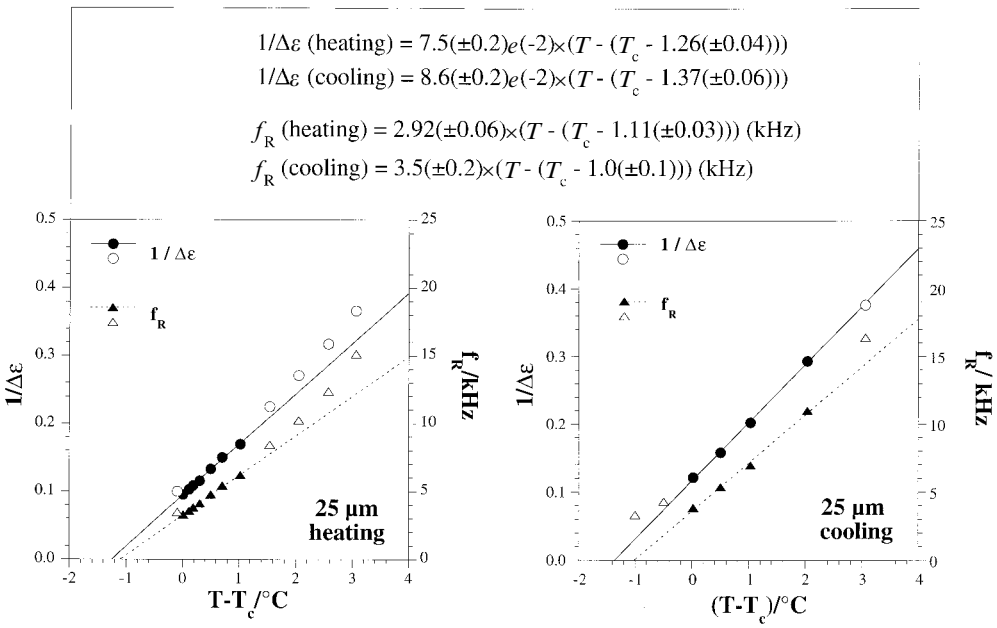

Figure 3. Relaxation frequency and inverse dielectric amplitude, as a function of temperature, for a 25 µm thick sample, on cooling and on heating. Linear expressions were fitted to the experimental data represented by full symbols. The expressions obtained are given above the graph.

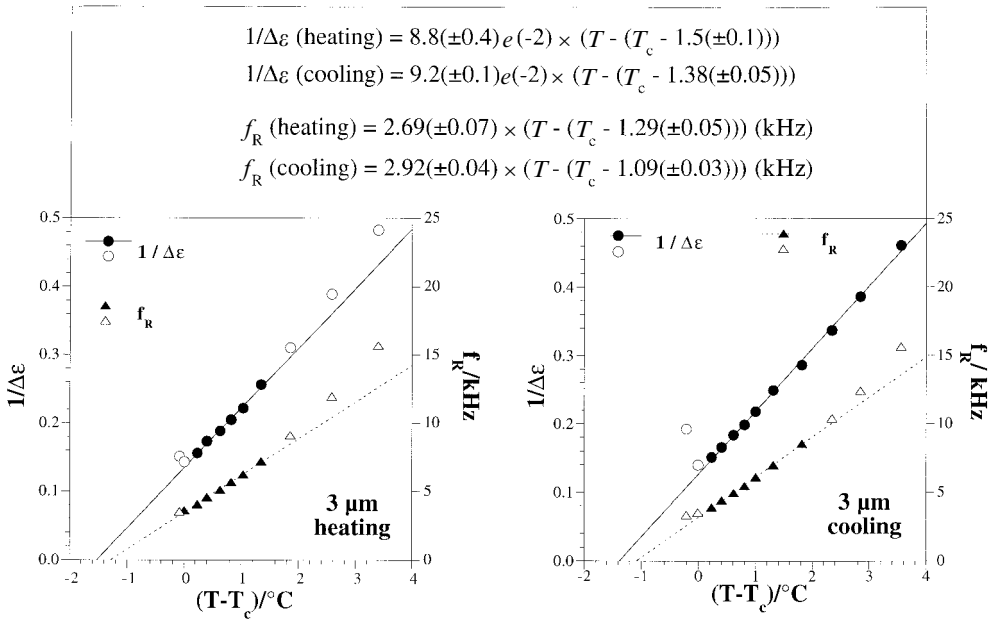

Figure 4. Relaxation frequency and inverse dielectric amplitude, as a function of temperature, for a 3 µm thick sample, on cooling and on heating. Linear expressions were fitted to the experimental data represented by full symbols. The expressions obtained are given above the graph.

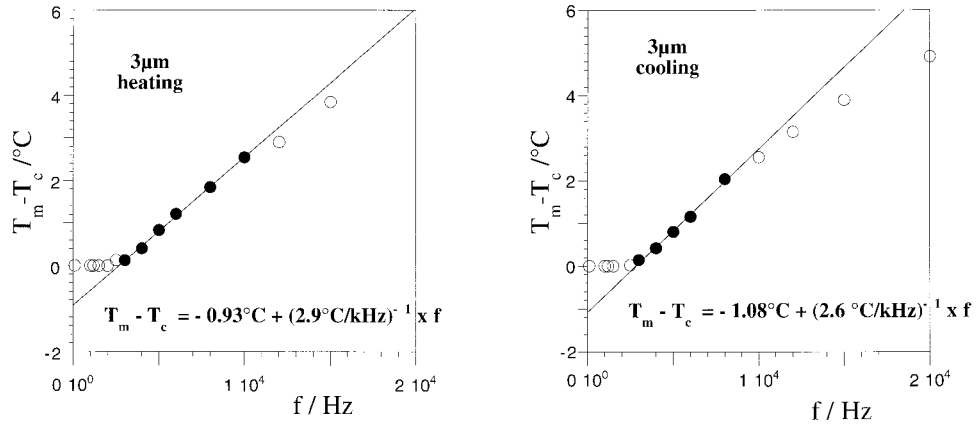

Figure 5. T_m as a function of the frequency, for a 3 µm thick sample.

of this alternative procedure is that it eliminates some of the errors introduced by the ITO electrodes and other spurious effects at high frequencies.

The strong increase in the dielectric amplitude of the soft mode, when approaching the SmA*–SmC$_A^*$ transition, indicates a tilt angle induced by the field. This compound presents a large electroclinic effect, as shown in figure 6. In the low temperature SmA* phase, a strong electric field induces an apparent tilt angle that can be nearly of the same order as the saturation tilt angle in the SmC$_A^*$ phase. For low values of E, the tilt angle varies linearly with the electric field in the SmA* phase. Above a certain value of the field, E_{lim}, the linear relation is no longer verified. An analogous behaviour was observed for the polarization, as shown in figure 7. It is obvious from figure 7 that in the SmA* phase E_{lim} decreases with decreasing temperature, on approaching the phase transition. The values of E_{lim} obtained from $D(E)$ curves for a 3 µm thick sample are presented in figure 8 (*a*), as a function of $T - T_c$. The values of E_{lim} obtained for this compound are rather high, when compared with the values of 0.4 V µm^{-1} (at $T_c + 2$ K) and

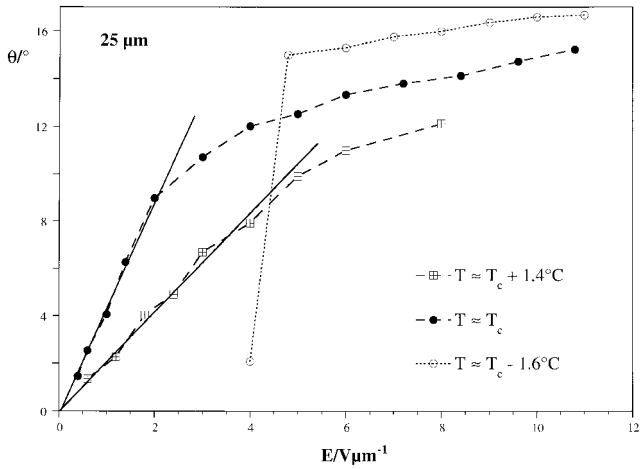

Figure 6. Measured tilt angle as a function of the applied field, at different temperatures, for a 25 µm thick sample. In the SmA* phase a linear regime is observed for low values of the measuring field. The full lines are merely a guide for the eye.

0.08 V µm^{-1} (close above T_c) obtained by Glogarová *et al.* [7] for a compound presenting a SmC*–SmA* phase transition.

The electroclinic coefficient, e, was determined from fittings to the linear part of the $\theta(E)$ curves. The linear behaviour of $1/e$ predicted by equation (6) was verified, as shown in figure 8 (*b*).

Using relations (6) and (7), we obtain:

$$\varepsilon' = \varepsilon_\infty + \chi_f C_f e.$$

The result of the linear fit of figure 8 (*c*) shows that $\varepsilon_\infty = 4.4 \pm 0.4$. This value is in good agreement with the high frequency dielectric constant observed during dielectric measurements. The table summarizes the most important results obtained from the fits to the experimental data. All the data presented in the table were obtained for a 3 µm thick sample on cooling runs. With the exception of

Table. Some numerical results obtained from fittings of theoretical expressions, for a 3 µm thick sample on cooling. $\langle T_s \rangle$ is the average of the temperatures T_s determined from different measurements.

$\chi_f C_f = 1.8 \times 10^8$ V m^{-1} rad^{-1}
$\alpha = 2.7 \times 10^4$ N m^{-2} rad^{-2} K^{-1}
$\gamma = 1.5$ Pa s
$\langle \overline{T_s} \rangle = T_c - 1.2$ K

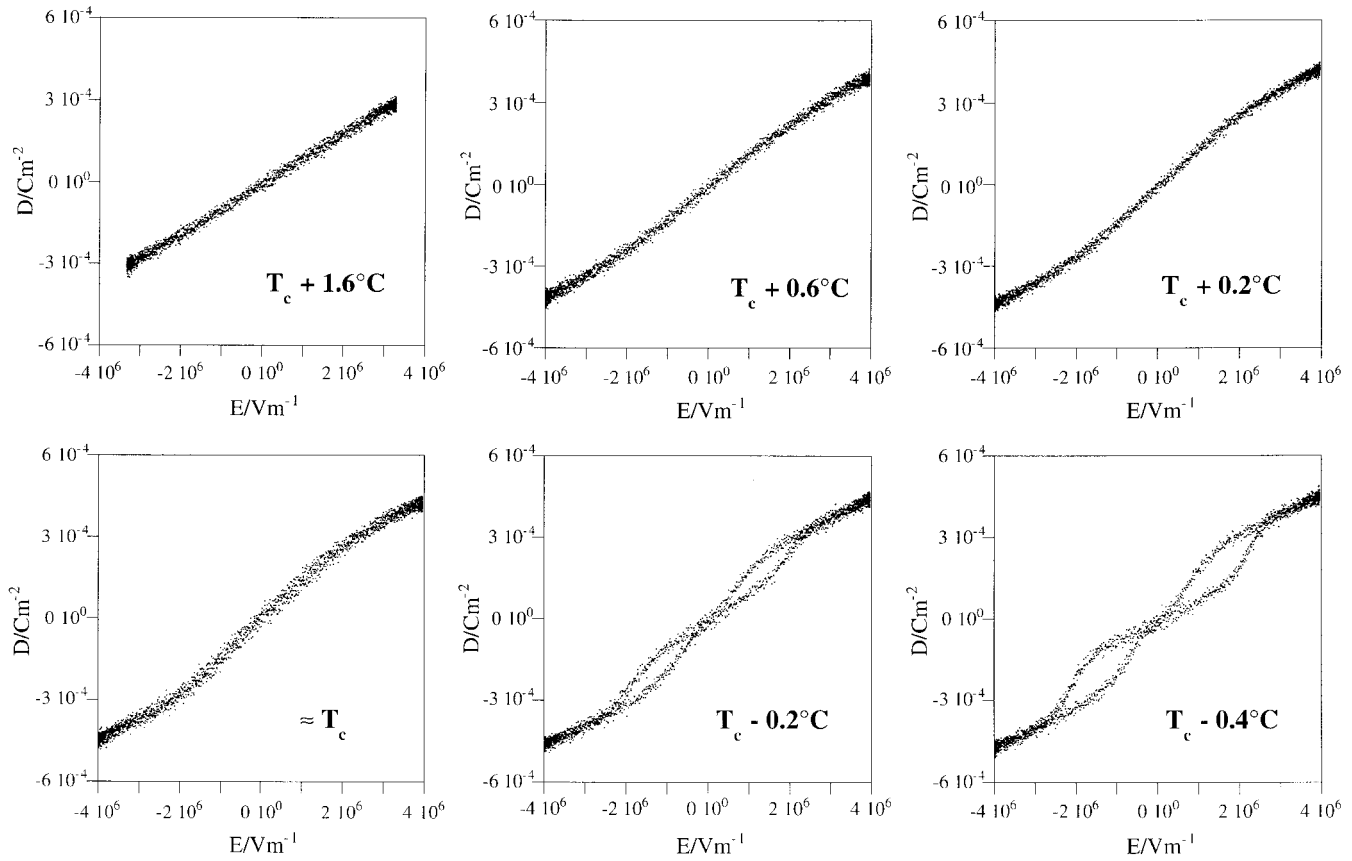

Figure 7. $D(E)$ curves obtained for a 3 µm thick sample, at several different temperatures.

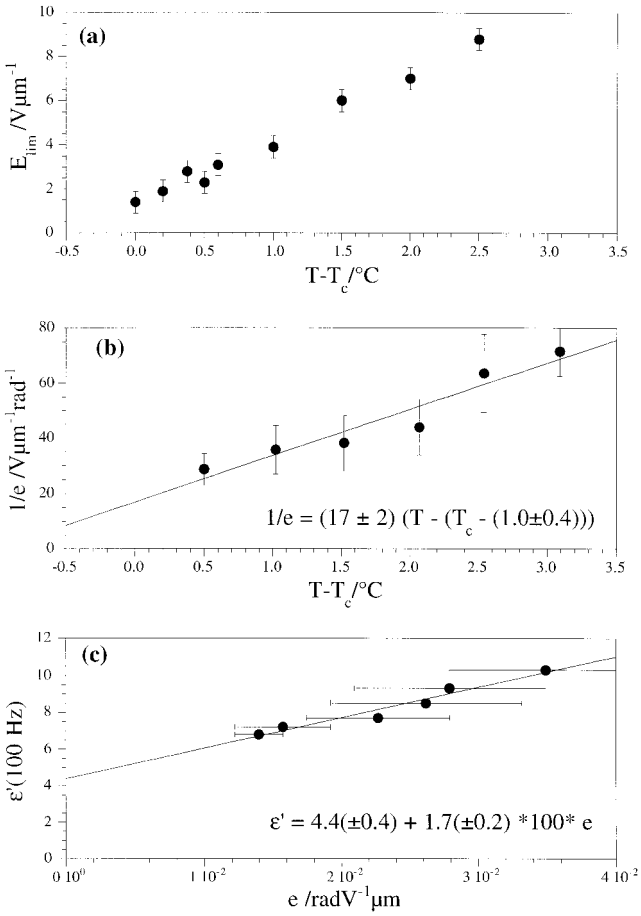

Figure 8. (*a*) Values of $E_{\lim}$ as a function of $T - T_c$. (*b*) Inverse electroclinic coefficient, $1/e = (\theta/E)^{-1}$, as a function of $T - T_c$. (*c*) Real part of the dielectric constant, ε', as a function of the electroclinic coefficient, $e = \theta/E$

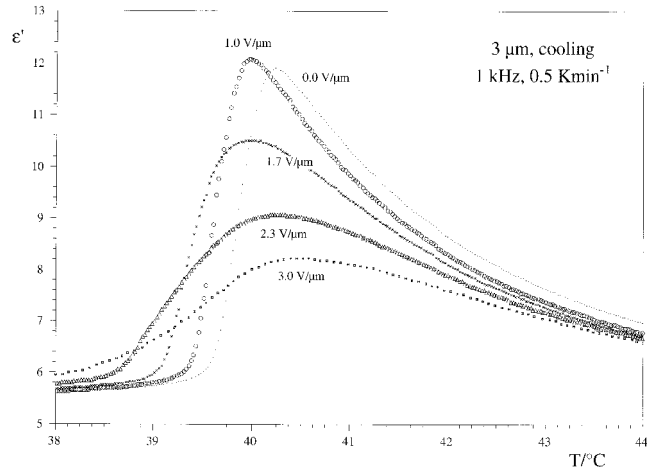

Figure 9. Real part of the dielectric constant, measured under different values of bias field, at 1 kHz, using a HP4192A and a 3 μm thick sample, on cooling runs.

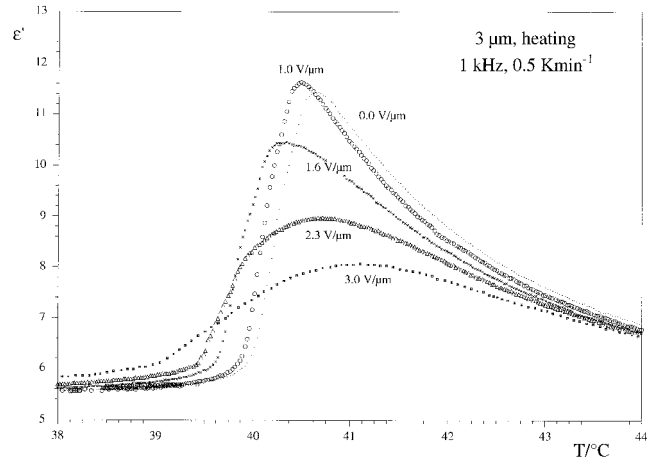

Figure 10. Real part of the dielectric constant, measured under different values of bias field, at 1 kHz, using a HP4192A and a 3 μm thick sample, on heating runs.

the viscosity coefficient, γ, which is very high, the values obtained for the different parameters are of the same order as those usually obtained for SmC*–SmA* phase transitions [6, 17].

4.1. *Dielectric measurements under bias field*

4.1.1. *Cooling/heating runs*

The dielectric constant was measured under different values of bias field ($0 < E_{d.c.} < 3$ V μm^{-1}), on cooling and heating runs. Figures 9 and 10 present some of the curves obtained at 1 kHz, using a HP4192A, on cooling and on heating runs, respectively. Similar curves were obtained at 100 Hz, with an Ando AG4311 bridge. The results obtained in both measurements are summarized in figure 11, where T_{max} and ε'_{max} are presented as functions of the bias field, on cooling and on heating. Figure 11 shows that we may distinguish two different regions. For bias field lower than $(E_{d.c.}/\text{V μm}^{-1})^{2/3} \approx 1$, ε'_{max} increases as T_{max} decreases; when $(E_{d.c.}/\text{V μm}^{-1})^{2/3} > 1.3$, the maximum value attained by the dielectric constant decreases further, but the temperature where it occurs increases with increasing bias field. This behaviour may be at least qualitatively understood with the help of the simplified model presented in § 2.

For $1 < (E_{d.c.}/\text{V μm}^{-1})^{2/3} < 1.3$, the observed behaviour probably corresponds to a transition between these two different regions and will not be discussed in detail.

For $(E_{d.c.}/\text{V μm}^{-1})^{2/3} < 1$, the ferroelectric amplitude mode of the SmA* phase should condense at $T_S = T_f + \varepsilon_o \chi_f C_f^2/\alpha$, but without bias field this softening is interrupted by the phase transition: the antiferroelectric order parameter ξ_a becomes non-zero below $T_c = T_S + 1.2$°C.

A small applied bias field induces a SmC structure in the SmA* phase and tends to unwind the helix in

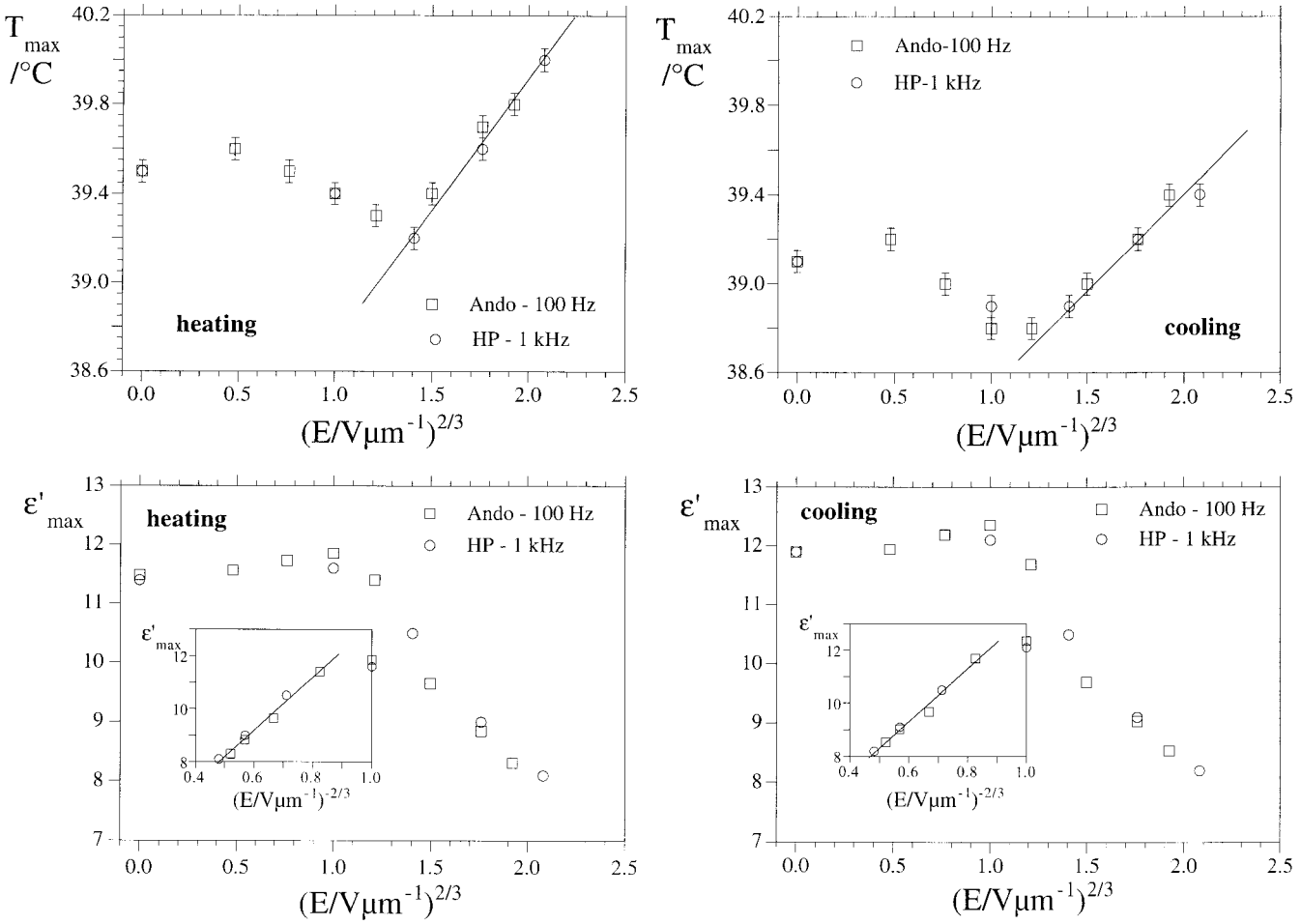

Figure 11. The maximum value of the dielectric constant, ε'_{max}, and the temperature where it occurs, T_{max}, are plotted as a function of $E^{2/3}$, for heating and cooling runs. The insets show the linear dependence of ε'_{max} on $E^{-2/3}$, for high values of the field. The lines are merely a guide for the eye.

the SmC^*_A phase. When the bias field is strong enough to unwind the helix completely, the antiferroelectric parameter becomes non-zero only below $T_a < T_c$. Therefore, as the bias field is increased, the SmA*–SmC^*_A phase transition temperature is decreased from $T_c = T_a + (2\Lambda_a q - K_a q^2)/\alpha$ $(q = \Lambda_a/K_a)$ to T_a, due to the unwinding of the helix. Optical observations of the texture have confirmed that an applied bias field decreases the transition temperature.

As the transition temperature decreases, the softening of the amplitude mode is visible until lower temperatures. Therefore, T_{max} decreases while $\varepsilon'_{max} = \varepsilon'[T_c(E)]$ increases slightly.

It should be noted that the temperature of the SmA*–SmC* phase transition also decreases with increasing bias field, due to the decrease in q. However, the maximum of the contribution of the soft mode can only be seen in the absence of the Goldstone mode. Previous studies of the SmA*–SmC* phase transition were performed with completely unwound samples ($q = 0$), and therefore this effect was not observed.

For $(E_{d.c.}/\text{V}\ \mu\text{m}^{-1})^{2/3} > 1.3$, from figure 8(*a*), we see that $E_{lim} \approx 1\ \text{V}\ \mu\text{m}^{-1}$ close to T_c. Above this value of the field, we are no longer in the linear regime at T_c. The b_f term in expansion (5) is no longer negligible and relations (12) should be approximately verified. According to these relations, the temperature where the maximum contribution of the soft mode occurs, T_{max}, will increase as $E^{2/3}$, while the maximum value of the dielectric constant will decrease as $E^{-2/3}$. This prediction is in good agreement with the behaviour of T_{max} and ε'_{max} observed in figure 11, for $(E_{d.c.}/\text{V}\ \mu\text{m}^{-1})^{2/3} > 1.3$.

At very high values of the bias field, a slight departure from the $E^{2/3}$ dependence is to be expected, since 6th order terms in E were neglected in the model. If the $\gamma_1(\Delta\xi_a)^2(\Delta\xi_f)^2$ were considered in expansion (5), the two order parameters would be coupled. The transition temperature to the SmC^*_A phase with $\xi_a \neq 0$, under high

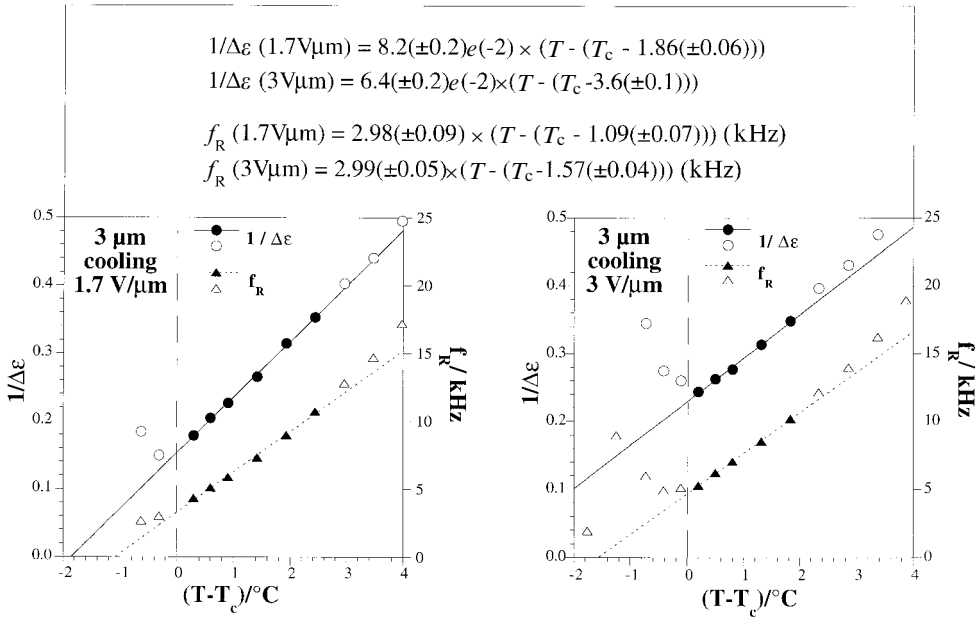

Figure 12. Relaxation frequency and inverse dielectric amplitude, as a function of temperature, obtained for a 3 μm thick sample, on cooling. T_c is the phase transition temperature for $E_{d.c.} = 0$. Linear expressions were fitted to the experimental data represented by full symbols. The expressions obtained are given above the graph.

bias field, continues to decrease with $E_{d.c.}^2$:

$$T_c = T_a + \frac{2\Lambda_a q - K_a q^2 - \gamma_1 \Delta\xi_f^2}{\alpha}$$

4.1.2. *Dielectric dispersion*

Figure 12 shows the relaxation frequency and inverse dielectric amplitude as a function of temperature, in the vicinity of T_c, for $E_{d.c.} = 1.7$ and 3 V μm^{-1}. According to our previous convention, T_c in these figures is the phase transition temperature for $E_{d.c.} = 0$. Comparing the fit results obtained for 3 μm thick samples, on cooling, for $E_{d.c.} = 0$ (figure 4) and for $E_{d.c.} = 1.7$ and 3 V μm^{-1} (figure 12), it is clear that the temperature where the linear fits cross the x axis decreases with increasing bias field. The $(\Delta\xi_f)^2$ term in equation (10) mimics a decrease in T_S.

The transition from the SmA* phase (or induced SmC structure) to the SmC_A^* phase at the temperature T_c is accompanied by a decrease in $\Delta\varepsilon$ and the corresponding increase in $1/\Delta\varepsilon$, which becomes too large to be represented in the main graph. The decrease of T_c with the applied bias field is seen in figures 4 and 12.

5. Conclusion

The compound studied presents a large electroclinic effect in the SmA* phase above the SmA*–SmC_A^* transition. In the region of linear regime, the experimental behaviour observed is analogous to that in reports by other authors for the SmA*–SmC* phase transition [6]. The viscosity coefficient γ is very high, but all other numerical values obtained for phenomenological coefficients are of the same order as those usually reported for compounds presenting the SmA*–SmC* phase transition [6, 17].

The presence of a strong Goldstone mode in the SmC* phase hides the peak of the soft mode contribution at T_c, which can only be observed in unwound samples. However, for a SmA*–SmC_A^* phase transition, the maximum dielectric contribution of the soft mode, at T_c, is easily observed without destroying the helicoidal structure of the SmC_A^* phase. Therefore, when dielectric measurements are performed as a function of the bias field, it is possible to observe at low fields the decrease of the phase transition temperature that is related to the suppression of the helix.

The authors are grateful to Dr J. P. Marcerou for enlightening discussions and to Dr M. Glogarová for providing useful bibliographic material. The authors also thank Albano Costa for his technical assistance. This work was supported by the project PRAXIS XXI/3/3.1/MMA/1769/95. S. Sarmento thanks project Praxis XXI for the grant BD/9545/96.

References

[1] Chandani, A. D. L., Gorecka, E., Ouchi, Y., Takezoe, H., and Fukuda, A., 1989, *Jpn. J. appl. Phys.*, **28**, 1265.

[2] Orihara, H., and Ishibashi, I., 1990, *Jpn. J. appl. Phys.*, **29,** L115.
[3] Cluzeau, P., Gisse, P., Ravaine, V., Levelut, A.-M., Barois, P., Huang, C. C., Rieutord, F., and Nguyen, H. T., 2000, *Ferroelectrics*, **244,** 1.
[4] Akizuki, T., Miyachi, K., Takanishi, Y., Ishikawa, K., Takezoe, H., and Fukuda, A., 1999, *Jpn. J. appl. Phys.*, **38,** 265.
[5] Hiraoka, K., Ouchi, Y., Takezoe, H., Fukuda, A., Inui, S., Kawano, S., Saito, M., Iwane, H., and Itoh, K., 1991, *Mol. Cryst. liq. Cryst.*, **199,** 197.
[6] Glogarovà, M., Destrade, Ch., Marcerou, J. P., Bonvent, J. J., and Nguyen, H. T., 1991, *Ferroelectrics*, **121,** 285.
[7] Glogarovà, M., and Pavel, J., 1989, *Liq. Cryst.*, **6,** 325.
[8] Nguyen, H. T., *et al.* (to be published).
[9] Beaubois, F., Faye, V., Marcerou, J. P., Nguyen, H. T., and Rouillon, J. C., 1999, *Liq. Cryst.*, **26,** 1351.
[10] Ema, K., Yao, H., Kawamura, I., Chan, T., and Garland, C. W., 1993, *Phys. Rev. E*, **47,** 1203.
[11] Žekš, B., and Čepič, M., 1993, *Liq. Cryst.*, **14,** 445.
[12] Lorman, V. L., Bulbitch, A. A., and Toledano, P., 1994, *Phys. Rev. E*, **49,** 1367.
[13] Orihara, H., and Ishibashi, I., 1995, *J. phys. Soc. Jpn.*, **64,** 3775.
[14] Gouda, F., Skarp, K., and Lagerwall, S. T., 1991, *Ferroelectrics*, **113,** 165.
[15] Yuzyuk, Y., Almeida, A., Sarmento, S., Simeão Carvalho, P., Pinto, F., Chaves, M. R., and Nguyen, H. T., 2000, *Ferroelectrics*, **239,** 181.
[16] Bourny, V., 1999, PhD thesis, Université de Picardie Jules Verne, France.
[17] Dupont, L., 1990, PhD thesis, Université de Bordeaux I, France.

Appendix

Derivation of relation (14)

The contribution of the amplitude mode (soft mode) to the real part of the dielectric constant, in the SmA* phase, is written as:

$$\varepsilon' = Re\left(\frac{\Delta\varepsilon_S}{1+\mathrm{i}\dfrac{\omega}{\omega_R}}\right) = \frac{\Delta\varepsilon_S}{1+\left(\dfrac{\omega}{\omega_R}\right)^2}$$

where $\omega_R = \alpha(T - T_S)/\gamma$ and $\Delta\varepsilon_S = \varepsilon_o(\chi_f C_f)^2/\alpha(T - T_S)$ as in relation (8). Substituting, we get:

$$\varepsilon' = \frac{\varepsilon_o(\chi_f C_f)^2\omega_R^2}{\alpha(T - T_S)(\omega_R^2 + \omega^2)} = \frac{\varepsilon_o(\chi_f C_f)^2\alpha(T - T_S)}{\alpha^2\dfrac{(T - T_S)^2}{\gamma^2} + \omega^2}.$$

For $\omega \geqslant \omega_R$, the function $\varepsilon'(T)$ presents a maximum at the temperature T_m where:

$$\left.\frac{\partial\varepsilon'}{\partial T}\right|_{T=T_m} = 0 \Leftrightarrow \omega^2 - \frac{(T_m - T_S)^2\alpha^2}{\gamma^2} = 0$$

$$\Rightarrow T_m = T_S + \frac{2\pi\gamma}{\alpha} \times f.$$